PCCP

PAPER

View Article Online
View Journal | View Issue

Cite this: *Phys. Chem. Chem. Phys.*, 2026, **28**, 8949

Study on translational diffusion of solute molecules in novel phosphonium-based dicationic ionic liquids by transient grating spectroscopy

Masaki Fujiwara, †[a] Shinya Okazoe,†[a] Sawaya Suzuki,[a] Koji Osawa,[b] Takatsugu Endo [b] and Yoshifumi Kimura *[a]

Translational diffusion coefficients of carbon monoxide (CO), diphenylacetylene (DPA), and diphenylcyclopropenone (DPCP) were determined by transient grating (TG) spectroscopy in five ionic liquids (ILs), including novel phosphonium-based dicationic ionic liquids (DILs): 1,6-bis(trioctylphosphonium)hexane bis(trifluoromethanesulfonyl)amide ($[(P_{888})_2C_6][NTf_2]_2$) and 1,10-bis(trioctylphosphonium)decane bis(trifluoromethanesulfonyl)amide ($[(P_{888})_2C_{10}][NTf_2]_2$). We tried to clarify the different effect of the alkyl-chain length comparing the diffusion coefficients in monocatinoic ILs and DILs with similar total number of alkyl carbons per charge of cation. Comparing two DILs, the viscosity of $[(P_{888})_2C_{10}][NTf_2]_2$ was smaller than that of $[(P_{888})_2C_6][NTf_2]_2$. Further, the X-ray scattering peak arising from the structural heterogeneity shifted to a larger q-value for the DIL of the longer linkage, indicating that the nonpolar domain became smaller for the DIL with the longer alkyl linkage. The diffusion coefficients of CO, DPA and DPCP in ILs were larger than those predicted by the Stokes–Einstein (SE) equation. In particular, the diffusion coefficient of CO in the phosphonium-based DILs deviated significantly from the SE prediction. Moreover, the degree of deviation was almost independent of the alkyl linkage chain length. By comparing the diffusion coefficients of CO in monocationic ILs and DILs, it was found that the diffusion coefficient of CO was correlated with the volume per charge of the cation.

Received 16th December 2025,
Accepted 17th March 2026

DOI: 10.1039/d5cp04887g

rsc.li/pccp

1. Introduction

Ionic liquids (ILs) are substances with melting points below 100 °C and are often composed of organic cations and inorganic anions. The properties of ILs vary dramatically by changing the combination of cations and anions. ILs have been explored for various applications: biological applications,[1] nanoparticle synthesis,[2] electrochemical reactions,[3] organic catalytic reactions,[4] and medium for energy storage.[5]

Imidazolium, pyrrolidinium, ammonium, and phosphonium are typically adopted as cations for ILs. Most of these cations contain both a polar part (charge centre) and a nonpolar part (alkyl chains). The existence of these two parts makes the structure of ILs unique. In particular, it has been suggested that a domain structure (or segregation between the polar and nonpolar parts) exists in ILs with long alkyl chains. First, the existence of segregation was proposed by computer simulations,[6,7] and then confirmed by structural analysis using X-ray or neutron scattering.[8,9] The structure of the cation can be easily tuned by elongating the alkyl chain length. A domain structure of IL not found in molecular liquids is induced by the balance of Coulomb interaction between constituent ions and hydrophobic interaction.[10] Elongation of alkyl chains increases the segregation of polar and nonpolar domains.

During the study on the structure of ILs, the dicationic IL (DIL), in which two cations are linked by a single alkyl chain, has received attention. It is interesting to determine how the structure and dynamics of DILs differ from those of monocationic ILs with similar alkyl chain lengths. In the case of DILs, the elongation of the alkyl linkage chain also enhances the domain structure.[11,12] Various types of DILs have been synthesized, and their physicochemical properties have been reported previously. Shirota *et al.* reported the relevance of the glass transition temperature (T_g) between dicationic and monocationic imidazolium-based ILs; glass transition temperature (T_g) of DILs with bis(trifluoromethanesulfonyl) amide) ($[NTf_2]^-$) was approximately 20 K higher than that of monocationic ILs.[13] Zhang *et al.* reported the thermal stability of ammonium DILs with the $[NTf_2]^-$ anion, evaluated by thermogravimetry; the thermal stability of DILs increased with longer linkage alkyl

[a] *Graduate School of Science and Engineering, Doshisha University, Kyotanabe-City, Kyoto 610-0321, Japan. E-mail: yokimura@mail.doshisha.ac.jp*
[b] *Faculty of Science and Engineering, Doshisha University, Kyotanabe-City, Kyoto 610-0321, Japan*
† M. F. and S. O. contributed equally.

chains among the same charge centre.[14] From the structural perspective, Li *et al.* proposed a unique assembly pattern of long linkage chains of DILs in micelle-like nanoaggregates. The flexibility of the linkage chains depends on their length, with longer chains adopting a bending structure, whereas the flexibility of shorter chains is restrained.[11] As shown in these examples, DILs have the potential to possess physicochemical properties or local structures that cannot be achieved by elongating the side alkyl chains on the monocation.

The molecular dynamics and chemical reactions in ILs are often affected by the existence of domain structures.[15] In this study, we focused on the translational diffusion coefficient of solutes in ILs. It has been repeatedly mentioned that the translational diffusion coefficients of non-charged molecules in ILs do not follow a simple hydrodynamics theory such as the Stokes–Einstein (SE) theory,

$$D = \frac{k_B T}{C\pi r\eta} \quad (1)$$

where D is the diffusion coefficient, k_B is the Boltzmann constant, T is the temperature, C is the boundary condition (slip: $C = 4$, stick: $C = 6$), η is the viscosity of the solvent, and r is the radius of the solute. Kaintz *et al.* reported the translational diffusion coefficients of neutral and ionic solutes in ordinary ILs using nuclear magnetic resonance (NMR) and analysed the deviation of the diffusion coefficients from the SE rule.[16] They indicated that the friction acting on the neutral solute molecule decreases from the prediction of the SE theory with a decrease in the relative size of the solute molecule compared to that of the solvent ions. Later, Kimura *et al.* added several data points, including a gaseous molecule (carbon monoxide, CO), using transient grating (TG) spectroscopy, and confirmed a similar trend.[17] Furthermore, they found that the deviation from the SE rule was more significant with an elongation of the alkyl chain length of the cation using phosphonium-based ILs. In contrast, the diffusion coefficients of diphenylcyclopropenone (DPCP) and diphenylacetylene (DPA) did not differ significantly. It is quite interesting to determine how these features appear in DILs, where the alkyl chain length per cation is twice that of the corresponding length of the monocation. However, a direct comparison of the diffusion dynamics between monocationic IL and DIL has not been performed until now to our best knowledge.

In this study, we evaluated the diffusion coefficients of CO, DPA, and DPCP in DILs with the same anion (bis(trifluoromethanesulfonyl)amide, $[NTf_2]^-$). Specifically, we prepared 1,6-bis(trioctylphosphonium)hexane NTf_2 ($[(P_{888})_2C_6][NTf_2]_2$) and 1,10-bis(trioctylphosphonium)decane NTf_2 ($[(P_{888})_2C_{10}][NTf_2]_2$), which are novel DILs, and 1,10-di(3-methylimidazolium-1-yl)decane NTf_2 ($[C_{10}(mim)_2][NTf_2]_2$) (Fig. 1). We compared the diffusion coefficients in dicationic ILs with those in monocationic ILs of similar total number of alkyl carbons per charge of cation. We found that the diffusion coefficient of CO was determined by the volume per charge of the cation, not by the volume of the cation itself, whereas the dicationic nature was a key factor for the diffusion of DPA and DPCP. Finally, we discuss the origin of the differences in the diffusion coefficients of the phosphonium-based DILs with respect to their domain structures.

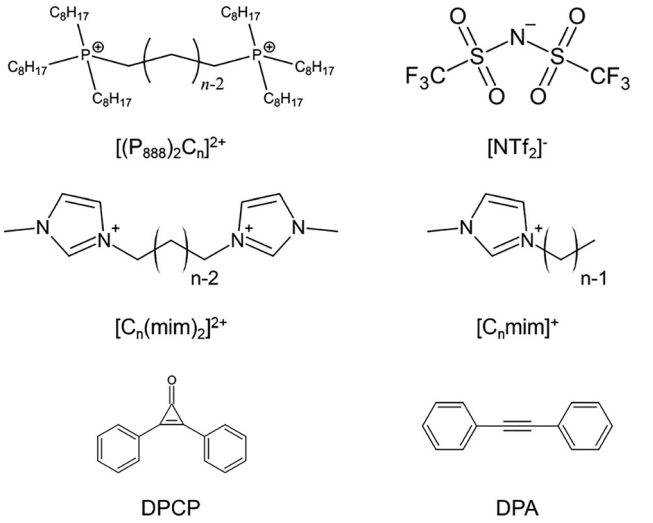

Fig. 1 Chemical structures of ILs and solute molecules used in this study.

2. Experimental

2.1 Materials

Trioctylphosphine (>95%) was purchased from Nippon Chemical Industrial Co., Ltd. 1,6-Dibromohexane (>97.0%) and 1,10-dibromodecane (>95.0%) were purchased from Tokyo Chemical Industry Co., Ltd. Methanol (>99.0%), dichloromethane (>99.5%), sodium bicarbonate (>99.6%), and bromocresol purple (BCP) were purchased from Nacalai Tesque. Sodium tetrafluoroborate ($Na[BF_4]$) (>98%) was purchased from STELLA CHEMIFA CORPORATION. Lithium NTf_2 (>99.8%) was purchased from KANTO CHEMICAL CO., INC. Chloroform-d containing 0.05 vol% tetramethylsilane and DPCP (>98.0%) were purchased from FUJIFILM Wako Pure Chemical Corporation. Distilled water was produced using RFD240HA (ADVANTEC). All chemicals were used as received, unless otherwise stated.

2.2 Nuclear magnetic resonance (NMR)

NMR measurements were performed using a JNM-ECA500 (JEOL). The ILs were dissolved in $CDCl_3$. The signal from tetramethylsilane (TMS) at 0 ppm was used as an internal reference for the ^{1}H NMR spectra. Residual signal from the solvent ($CHCl_3$) at 77.16 ppm for the ^{13}C NMR was used as an internal reference 18.

2.3 Mass spectroscopy (MS)

MS spectroscopy was performed using a timsTOF (IMS-QTOF, Bruker). The methanol solution of IL was injected into the liquid chromatography and ionized by electrospray ionization. Positive ions were detected to confirm the cation structure.

2.4 Synthesis of $[(P_{888})_2C_6][BF_4]_2$

Trioctylphosphine (65.0 g, 175 mmol) was added to 1,6-dibromohexane (15.1 g, 61.9 mmol) and kept at 343 K for

16 h under a nitrogen atmosphere. Trioctylphosphine (21.0 g, 56.7 mmol) and hexane (50 mL) were added to the crude reaction mixture and maintained at 343 K for 29 h under a nitrogen atmosphere. Solid samples were collected from the crude sample and washed with hexane. The solid sample was evacuated to remove hexane and dissolved in dichloromethane. $Na[BF_4]$ (32.0 g, 290 mmol) was dissolved in distilled water and filtrated to remove impurities not dissolved in water. After mixing the solution vigorously, the dichloromethane layer was separated and washed with distilled water to obtain $[(P_{888})_2C_6][BF_4]_2$. $[(P_{888})_2C_6][BF_4]_2$ was purified by recrystallization from methanol several times.

Chemical formula: $C_{54}H_{114}F_8B_2P_2$, M_w: 999.04, ^{1}H NMR (500 MHz, $CDCl_3$): δ_H ppm: 2.15(m, 16H), 1.60(m, 8H), 1.49(m, 24H), 1.29(m, 48H), 0.88(t, 7 Hz, 18H), $^{13}C\{^1H\}$ NMR (126 MHz, $CDCl_3$): δ_C ppm: 31.60, 30.59(d, J_{P-C} = 14 Hz), 28.88, 28.72, 22.49, 21.46(d, J_{P-C} = 5 Hz), 20.12(d, J_{P-C} = 4 Hz), 18.49(d, J_{P-C} = 48 Hz), 18.37(d, J_{P-C} = 47 Hz), 13.94, $^{31}P\{^1H\}$ NMR (202 MHz, $CDCl_3$): δ_P ppm: 33.39, ^{19}F NMR (470 MHz, $CDCl_3$): δ_F ppm: −150.81, elemental analysis: calcd. for $C_{54}H_{114}F_8B_2P_2$: C 64.92, H 11.50, F 15.21; found: C 64.80, H 11.76, F 13.47, MS (ESI): calcd. for $[(P_{888})_2C_6]^{2+}$ ($C_{54}H_{114}P_2{}^{2+}$, [M]), 412.4193; found, 412.4191. The component of F in elemental analysis was somewhat lower than that of calculated because of incomplete combustion. Bromide was not detected by elemental analysis.

2.5 Synthesis of $[(P_{888})_2C_6][NTf_2]_2$

$[(P_{888})_2C_6][BF_4]_2$ (1.61 g, 1.61 mmol) was dissolved in dichloromethane, and $Li[NTf_2]$ (1.64 g, 5.71 mmol) was dissolved in distilled water. After mixing the solution vigorously, the dichloromethane layer was separated and washed with distilled water to obtain $[(P_{888})_2C_6][NTf_2]_2$.

Chemical formula: $C_{58}H_{114}N_2F_{12}O_8P_2S_4$, M_w: 1385.72, ^{1}H NMR (500 MHz, $CDCl_3$): δ_H ppm: 2.17(m, 4H), 2.06(m, 12H), 1.58(s, 8H), 1.47(m, 24H), 1.27(m, 48H), 0.88(t, 7 Hz, 18H), $^{13}C\{^1H\}$ NMR (126 MHz, $CDCl_3$): δ_C ppm: 119.79(q, J_{C-F} = 321 Hz), 31.49, 30.35(d, J_{P-C} = 15 Hz), 29.05(d, J_{P-C} = 15 Hz), 28.75, 28.50, 22.40, 21.24(d, J_{P-C} = 4 Hz), 20.71(d, J_{P-C} = 4 Hz), 18.38(d, J_{P-C} = 47 Hz), 18.33(d, J_{P-C} = 48 Hz), 13.81, $^{31}P\{^1H\}$ NMR (202 MHz, $CDCl_3$): δ_P ppm: 33.47, ^{19}F NMR (470 MHz, $CDCl_3$): δ_F ppm: −78.70, elemental analysis: calcd. for $C_{58}H_{114}N_2F_{12}O_8P_2S_4$: C 50.27, H 8.29, N 2.02, F 16.45, S 9.26; found: C 50.07, H 8.26, N 1.94, F 16.48, S 9.13, MS (ESI): calcd. for $[(P_{888})_2C_6]^{2+}$ ($C_{54}H_{114}P_2{}^{2+}$, [M]), 412.4193; found, 412.4190. Weak signals from impurities were detected in the ^{31}P NMR spectrum (Fig. S1).

2.6 Synthesis of $[(P_{888})_2C_{10}][BF_4]_2$

Trioctylphosphine (42.2 g, 114 mmol) and 1,10-dibromodecane (10.2 g, 33.9 mmol) were added to hexane (100 mL) and kept at 343 K for 90 h under a nitrogen atmosphere. The crude sample was evacuated and dissolved in dichloromethane. $Na[BF_4]$ (18.4 g, 166 mmol) was dissolved in distilled water and filtrated to remove impurities not dissolved in water. After mixing the solution vigorously, the dichloromethane layer was separated and washed with distilled water to obtain $[(P_{888})_2C_{10}][BF_4]_2$. $[(P_{888})_2C_{10}][BF_4]_2$ was purified by recrystallization from methanol several times.

Chemical formula: $C_{58}H_{122}F_8B_2P_2$, M_w: 1055.15, ^{1}H NMR (500 MHz, $CDCl_3$): δ_H ppm: 2.16(m, 16H), 1.50(m, 32H), 1.28(m, 56H), 0.88(t, 7 Hz, 18H), $^{13}C\{^1H\}$ NMR (126 MHz, $CDCl_3$): δ_C ppm: 31.76, 30.74(d, J_{P-C} = 15 Hz), 30.32(d, J_{P-C} = 15 Hz), 29.03, 28.89, 28.50, 22.65, 21.64(d, J_{P-C} = 5 Hz), 21.26(d, J_{P-C} = 4 Hz), 18.60(d, J_{P-C} = 47 Hz), 18.55(d, J_{P-C} = 47 Hz), 14.13, $^{31}P\{^1H\}$ NMR (202 MHz, $CDCl_3$): δ_P ppm: 33.55, ^{19}F NMR (470 MHz, $CDCl_3$): δ_F ppm: −151.06, elemental analysis: calcd. for $C_{58}H_{122}F_8B_2P_2$: C 66.03, H 11.66, F 14.40; found: C 65.99, H 11.56, F 11.19, MS (ESI): calcd. for $[(P_{888})_2C_6]^{2+}$ ($C_{58}H_{122}P_2{}^{2+}$, [M]), 440.4506; found, 440.4505. The component of F in elemental analysis was somewhat lower than that of calculated because of incomplete combustion. Bromide was not detected by elemental analysis.

2.7 Synthesis of $[(P_{888})_2C_{10}][NTf_2]_2$

$[(P_{888})_2C_{10}][BF_4]_2$ (1.70 g, 1.61 mmol) was dissolved in dichloromethane and $Li[NTf_2]$ (1.69 g, 5.89 mmol) was dissolved in distilled water. After mixing the solution vigorously, the dichloromethane layer was separated and washed with distilled water to obtain $[(P_{888})_2C_{10}][NTf_2]_2$.

Chemical formula: $C_{62}H_{122}F_{12}O_8P_2S_4$, M_w: 1441.83, ^{1}H NMR (500 MHz, $CDCl_3$): δ_H ppm: 2.09(m, 16H), 1.47(m, 32H), 1.28(m, 56H), 0.88(t, 7 Hz,18H), $^{13}C\{^1H\}$ NMR (126 MHz, $CDCl_3$): δ_C ppm: 119.75(q, J_{C-F} = 321 Hz), 31.42, 30.24(d, J_{P-C} = 14 Hz), 30.19(d, J_{P-C} = 14 Hz), 28.66, 28.43, 28.11, 22.34, 21.18(d, J_{P-C} = 5 Hz), 21.09(d, J_{P-C} = 5 Hz), 18.32(d, J_{P-C} = 48 Hz), 18.27(d, J_{P-C} = 48 Hz), 13.75, $^{31}P\{^1H\}$ NMR (202 MHz, $CDCl_3$): δ_P ppm: 33.51, ^{19}F NMR (470 MHz, $CDCl_3$): δ_F ppm: −78.70, elemental analysis: calcd. for $C_{62}H_{122}F_{12}O_8P_2S_4$: C 51.65, H8.53, N 1.94, F 15.81, S 8.90; found: C 51.99, H 8.60, N 1.84, F 15.62, S 8.60, MS (ESI): calcd. for $[(P_{888})_2C_6]^{2+}$ ($C_{58}H_{122}P_2{}^{2+}$, [M]), 440.4506; found, 440.4503. Weak signals from impurities were detected in the ^{31}P NMR spectrum (Fig. S2).

2.8 Synthesis of imidazolium ILs

Imidazolium-based ILs $[C_n\text{mim}][NTf_2]$ (n = 5, 10) and $[C_{10}(\text{mim})_2][NTf_2]_2$ were synthesized following previously reported procedures.[19,20]

2.9 X-ray scattering

X-ray scattering measurements were conducted at room temperature using a NANO-Viewer (Rigaku, λ_{probe} = 0.15418 nm) at a voltage of 40 kV and a filament current of 30 mA.[21] The exposure time was set to 60 min to exclude the noise. The scattering signal was detected using a 2-dimensional detector (PILATUS 100 K), and a 1-dimensional pattern was generated by integrating the 2D data. For the measurement of dynamics and structure, the ILs were evacuated for 24 h at 343 K. Residual water content thus prepared was typically less than 50 ppm determined by Karl Fischer titration.

2.10 Differential scanning calorimetry (DSC)

DSC measurements were performed using a DSC7020 (Hitachi). The samples for DSC measurements were evacuated for 16 h at 343 K. Approximately 10 mg of the sample was loaded into an

aluminum sample pan under an argon atmosphere. The temperature was varied from 353 K to 253 K (for $[(P_{888})_2C_6][BF_4]_2$ and $[(P_{888})_2C_{10}][BF_4]_2$) and from 323 to 173 K (for $[(P_{888})_2C_6][NTf_2]_2$ and $[(P_{888})_2C_{10}][NTf_2]_2$) at a scanning rate of 5 K min^{-1}.

2.11 Viscosity

The viscosity was measured using a DV-II+Pro (BROOKFIELD) from 298 to 323 K, and using a CAP2000+ (BROOKFIELD) above 323 K.

2.12 Transient grating (TG) spectroscopy

The experimental setup for the TG experiments has been described elsewhere.[17] Briefly, the third-harmonic output (λ_{pump} = 355 nm) from a pulsed Nd:YAG laser (Minilite; Continuum) was used as the excitation pulse, which was divided into two pulses using a beamsplitter. The pulses were simultaneously introduced into the sample cell at a particular angle (2θ) to produce an optical transient grating in the sample. DPCP photodissociates[22,23] at the bright fringe of the optical grating to produce thermal and population gratings of CO, DPA, and DPCP, which modulate the refractive index of the solution.

$$\text{DPCP} \rightarrow \text{DPA} + \text{CO} \quad (2)$$

These sinusoidal modulations were observed through the diffraction of the continuous-wave output of a 633-nm He–Ne laser (LGK-7654-8; LASOS) introduced into the sample solution under Bragg diffraction conditions. The diffracted light (TG signal) was detected using a photomultiplier and transferred to an oscilloscope (DSO-X 2014A; Agilent). The signal decay, which corresponds to thermal and molecular translational diffusion across the grating fringe, was transferred to a computer for analysis. The temperature of the sample solution was controlled using a Peltier temperature controller (VPE-20, VICS Co.) with a homemade cell holder.

The experiments were conducted as follows. The TG signal of the BCP solution in methanol was first acquired at a particular excitation pulse crossing angle at room temperature to determine the amplitude of the grating wavenumber q, which is required for the TG signal analysis, as described later. The value of q is given by the following equation:

$$q = \frac{4\pi \sin\theta}{\lambda} = \frac{2\pi}{\Lambda} \quad (3)$$

where Λ is the grating spacing. Subsequently, the TG signals of the DPCP solution in the IL were acquired under the same experimental conditions. This series of experiments was conducted at various excitation pulse angles and temperatures. The repetition rate of the laser was adjusted from 5 to 0.1 Hz, depending on the viscosity of the solvent.

All ILs were dried for at least 12 h at 333 K under vacuum before preparing the sample solutions by adding DPCP at a concentration of approximately 15 mM. For the TG measurements, the sample solutions were sealed in 1-cm quartz cells under vacuum.

3. Results

3.1 Physicochemical properties of DILs

The X-ray scattering patterns of the phosphonium-based DILs exhibited three peaks, as shown in Fig. 2. This result is consistent with previous reports for phosphonium-based monocationic ILs with the NTf_2 anion.[24,25] The highest and middle q peaks were assigned to the adjacency and charge alternation of the cations and anions, respectively. The highest q peak was almost independent of the alkyl linkage chain length of the DILs. The average distance separating two like-charge ions was calculated using eqn (3) to be 8.9 Å for $[(P_{888})_2C_6][NTf_2]_2$ and 9.0 Å for $[(P_{888})_2C_{10}][NTf_2]_2$. The lowest q peak originates from the alternation of polar and nonpolar regions, which is related to the structural heterogeneity of ILs. This peak generally shifted toward smaller q with increasing alkyl chain length of the phosphonium-based ILs. However, as shown in Fig. 2, the opposite tendency was observed for the alkyl linkage chain of phosphonium-based DILs, indicating that shorter alkyl linkage chains resulted in larger nonpolar domains ($[(P_{888})_2C_6][NTf_2]_2$: 17.6 Å, $[(P_{888})_2C_{10}][NTf_2]_2$: 14.9 Å).

Fig. 3 shows the DSC profiles of the cooling and heating of (a) $[(P_{888})_2C_6][NTf_2]_2$ and (b) $[(P_{888})_2C_{10}][NTf_2]_2$. The glass transition temperatures were observed at approximately 208 and 205 K for $[(P_{888})_2C_6][NTf_2]_2$ and $[(P_{888})_2C_{10}][NTf_2]_2$. Namely, $[(P_{888})_2C_6][NTf_2]_2$ and $[(P_{888})_2C_{10}][NTf_2]_2$ are liquid state at room temperature. Other phase transitions, except for the glass transition, were not observed during the cooling and heating processes in the three cycles. DSC profiles of $[(P_{888})_2C_6][BF_4]_2$ and $[(P_{888})_2C_{10}][BF_4]_2$ are shown in Fig. S3. Clear phase transitions were observed for $[(P_{888})_2C_6][BF_4]_2$, and the melting temperature was estimated as 334 K. On the other hand, no clear phase transition was detected for $[(P_{888})_2C_{10}][BF_4]_2$.

Fig. 4 shows the temperature dependence of the viscosity of $[(P_{888})_2C_n][NTf_2]_2$ (n = 6, 10). Fig. S4 shows the results for $[C_nmim][NTf_2]$ (n = 5, 10) and $[C_{10}(mim)_2][NTf_2]_2$. By fitting the Vogel–Fulcher–Tammann (VFT) equation, we determined the VFT parameters, η_0, B, and T_0 for each IL (Table S4).

$$\ln\eta = \ln\eta_0 + \frac{B}{T - T_0} \quad (4)$$

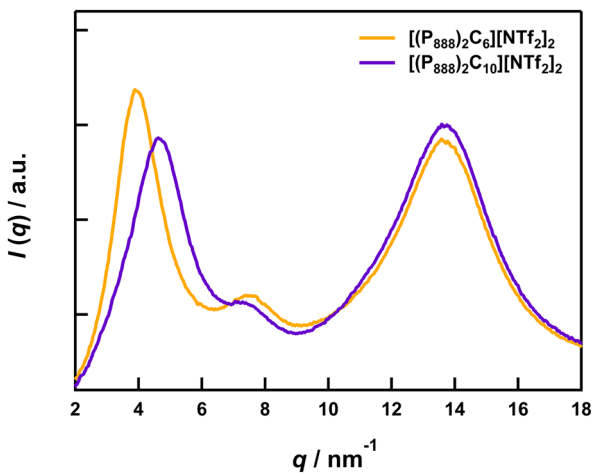

Fig. 2 X-ray scattering patterns of $[(P_{888})_2C_n][NTf_2]_2$ (n = 6, 10) at 298 K.

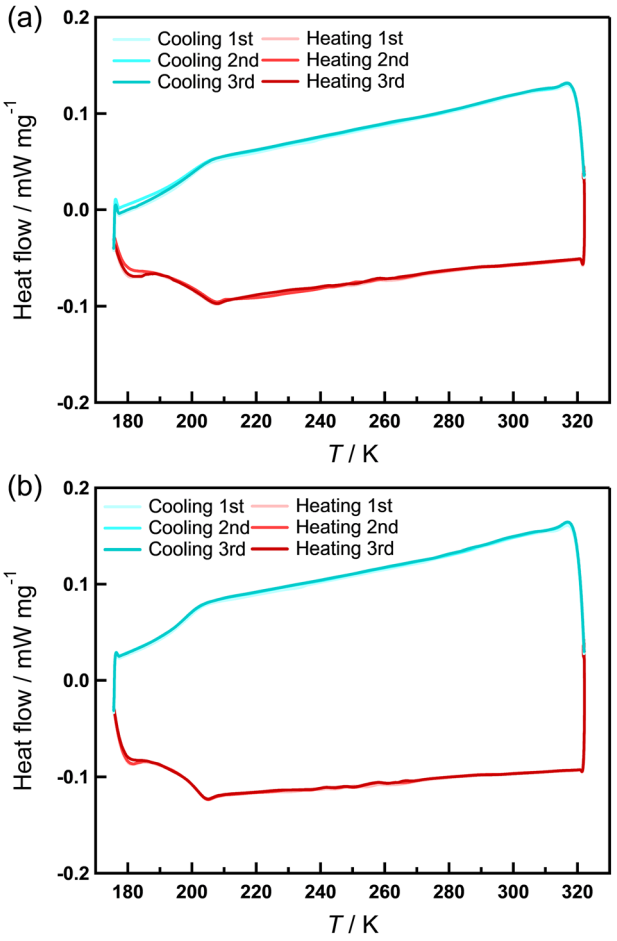

Fig. 3 DSC profiles of (a) $[(P_{888})_2C_6][NTf_2]_2$ and (b) $[(P_{888})_2C_{10}][NTf_2]_2$ scanned at 5 K min^{-1}.

For phosphonium-based DILs, the DIL with the shorter alkyl linkage chain exhibited higher viscosities than that with the longer chains, which is the opposite trend observed for phosphonium-based monocationic ILs.[26,27] For imidazolium-based ILs, $[C_{10}(mim)_2][NTf_2]_2$ exhibited higher viscosity than $[C_n mim][NTf_2]$ (n = 5, 10).

3.2 Diffusion coefficients

The intensity of the TG signal is expressed by the following equation:[28,29]

$$I_{TG}(t) = \alpha[\delta n_{th}(t) + \delta n_{spe}(t)]^2 \quad (5)$$

where δn_{th} and δn_{spe} are the refractive index changes due to the thermal (thermal grating) and the chemical species (species grating). In the present system, the TG signal contains both refractive index changes from thermal and from three chemical species (eqn (2)). The signal intensity is, therefore, expressed by the following equation.[30]

$$I_{TG}(t) = \alpha[\delta n_{th}\exp(-D_{th}q^2t) + \delta n_{CO}\exp(-D_{CO}q^2t) + \delta n_{DPA}\exp(-D_{DPA}q^2t) + \delta n_{DPCP}\exp(-D_{DPCP}q^2t)]^2 \quad (6)$$

Since the decay rate $D_{th}q^2$ of the thermal grating is significantly faster than those of the other three components, only the species grating was analyzed for imidazolium-based ILs.

Fig. 5 shows the TG signals obtained from $[C_5mim][NTf_2]$, $[C_{10}mim][NTf_2]$, and $[C_{10}(mim)_2][NTf_2]_2$. At the same grating wavenumber q^2, the timescale for the complete decay of the TG signal was one order of magnitude slower in the DIL $[C_{10}(mim)_2][NTf_2]_2$, which was attributed to its high viscosity. By altering the crossing angle 2θ of the pump pulses, we performed the measurements at various q^2 values (see eqn (3)) to determine the diffusion coefficients. Fig. 6 shows a typical example of plotting the decay rates $D_i q^2$ of each component against q^2. The value of q^2 was determined by measuring the decay rate of the thermal grating of a methanol solution of BCP at the same optical geometry. The diffusion coefficients were obtained from the slope of the plot shown in Fig. 5. The above procedures were performed at different temperatures to obtain the diffusion coefficients at each temperature (Table S5).

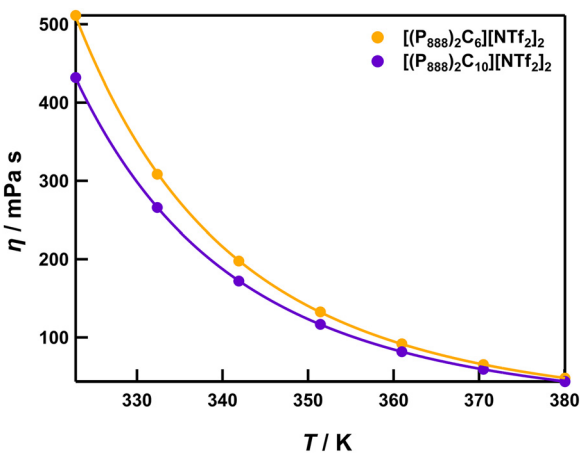

Fig. 4 Viscosity η of $[(P_{888})_2C_n][NTf_2]_2$ (n = 6 and 10) as a function of temperature T. The solid lines represent the fitting curves obtained using eqn (4).

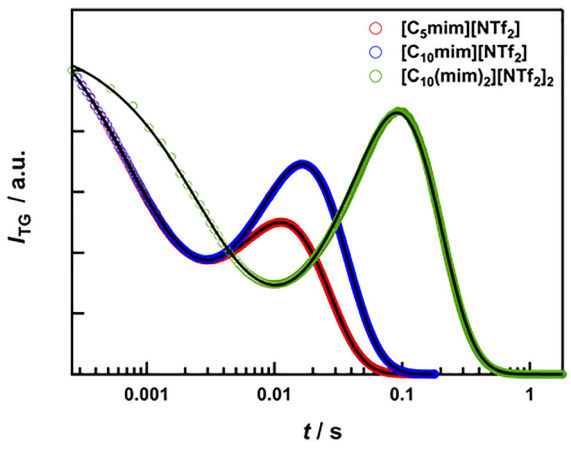

Fig. 5 Typical TG signals in $[C_5mim][NTf_2]$, $[C_{10}mim][NTf_2]$, and $[C_{10}(mim)_2][NTf_2]_2$ at 312 K and q^2 = 1.4 μm^{-2}. The horizontal axis is logarithmic in scale. Signal intensities are normalized at 2.6 × 10^{-3} s. The solid lines represent the best fitting-curves.

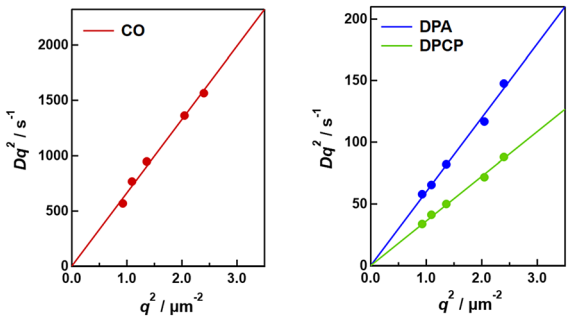

Fig. 6 q^2 dependence of the decay rate constants of the species grating signals of CO, DPA, and DPCP in [C_5mim][NTf_2] at 312 K.

Fig. 7 shows the TG signal obtained from $[(P_{888})_2C_n][NTf_2]_2$ (n = 6, 10). Because the thermal diffusivities of these ILs have not been reported, we fitted the TG signal using eqn (6), including the thermal grating decay. Similar to imidazolium-based ILs, TG signals were measured at various q^2, and a typical example of plotting the decay rate $D_i q^2$ against q^2 is shown in Fig. S5. Measurements were performed at different temperatures. Table S6 lists the diffusion coefficients of each solute molecule at each temperature. At all measured temperatures, D_{th} of $[(P_{888})_2C_{10}][NTf_2]_2$ was larger than that of $[(P_{888})_2C_6][NTf_2]_2$.

4. Discussion

4.1 Physicochemical properties of DILs

In this section, we compare the T_g, η, and X-ray scattering patterns of phosphonium-based DILs with those of monocationic ILs or imidazolium-based DILs. Yao *et al.* reported T_g of several phosphonium-based monocationic ILs with NTf_2 anion; the T_g values of $[P_{666n}][NTf_2]$ (for n = 2, 6, 8, and 12) were around 185 K and around 195 K (for n = 14).[31] In the case of phosphonium-based monocationic IL with octyl chains, that of $[P_{8888}][NTf_2]$ was 184.7 K.[32] The T_g values of $[(P_{888})_2C_6][NTf_2]_2$ and $[(P_{888})_2C_{10}][NTf_2]_2$ were around 205 K, and these were higher than those of monocationic ILs above mentioned and comparable to that of the other phosphonium-based dicationic IL, $[(P_{666})_2C_{10}][NTf_2]_2$ (T_g = 205 K).[33] This trend is consistent with the case of imidazolium-based ILs as reported previously.[13]

As the alkyl linkage chain of imidazolium-based DILs increases, the viscosity η increases[13] and the X-ray scattering peak arising from the structure heterogeneity shifts to a smaller q-value indicating that the nonpolar domain grows larger.[11] These results are consistent with those for monocationic ILs.[13] Interestingly, the phosphonium-based DILs synthesized in this study exhibited the opposite trend. As shown in Fig. 2 and 4, as the alkyl linkage chain of $[(P_{888})_2C_n][NTf_2]_2$ became longer, the viscosity decreased and the nonpolar domain increased. Although several aggregation models have been proposed for the nanoscale structure of DILs,[11] the observed trend in this study cannot be explained using conventional models. One plausible reason is the difference in the role of the alkyl linkage chain. The alkyl linkage chain attached to the imidazolium-based DILs is the only alkyl carbon capable of forming a nonpolar domain. In contrast, phosphonium-based DILs have six unbridged alkyl chains that can form heterogeneous structures. Hence, the alkyl linkage chain exhibits flexibility between the nonpolar domains. This enhanced flexibility likely manifests as microscopically well-folded nonpolar domains and macroscopically low viscosity. In practical expressions, earphones in your pocket are more likely to be knotted when the cord is longer, making them harder to untangle.[34,35] In the following section, we discuss the diffusion coefficients with respect to the structure. Although the temperatures are slightly higher than the temperature at which the X-ray scattering measurements were performed, the structure of ILs hardly changes with temperature unless the phase-transition occurs.[36–38]

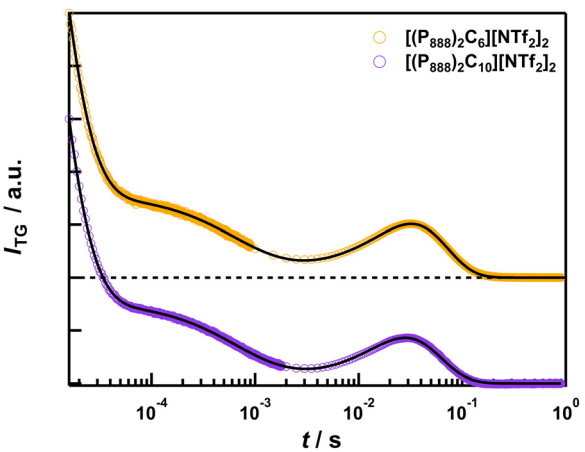

Fig. 7 Typical TG signals in $[(P_{888})_2C_6][NTf_2]_2$ and $[(P_{888})_2C_{10}][NTf_2]_2$ at 331 K and q^2 = 1.2 μm^{-2}. The horizontal axis is logarithmic in scale. Signal intensities are normalized at 1.6 × 10^{-5} s. The solid lines represent the best fitting-curves.

4.2 Diffusion coefficients

Fig. 8 shows the diffusion coefficients of CO, DPA, and DPCP plotted against $T\eta^{-1}$. The broken lines in the figure represent the predictions from the SE equation theory with stick boundary condition (C = 6). In the calculation, the radii of CO, DPA and DPCP were assumed to be 1.86, 3.50, and 3.54 Å, respectively, as in the previous paper.[17] The viscosity values at different temperatures were estimated from the VFT theory (eqn (4)). Although the diffusion coefficients of all solutes in all ILs studied here increased with $T\eta^{-1}$, the values were larger than those predicted from the SE equation. The deviation was very large for the smallest solute, CO, as already shown previously, and the dependence was not linear, in contrast to the prediction from the SE theory. Empirically the dependence was well simulated by the power law of (T/η) as:[17]

$$D = \left(D_0/\mathrm{m^2\ s^{-1}}\right)\left(\frac{(T/\mathrm{K})}{(\eta/\mathrm{mPa\ s})}\right)^{\alpha} \quad (7)$$

where D_0 and α are constants inherent to the solute and solvent, respectively. α represents the viscosity dependence of the diffusion coefficient, and the equation corresponds to the SE relationship when α = 1. Tables S7–S9 summarized the values of

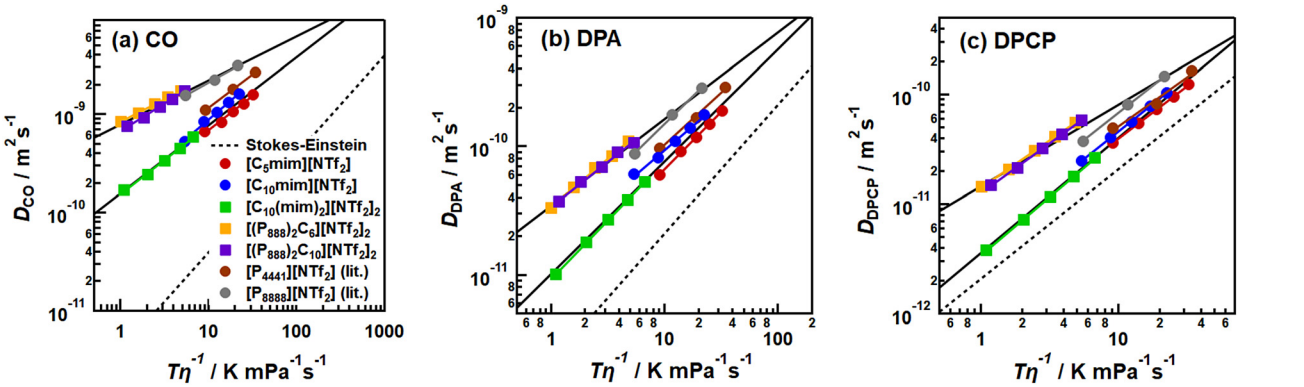

Fig. 8 Diffusion coefficients of (a) CO, (b) DPA, and (c) DPCP as function of $T\eta^{-1}$. Both scales are logarithmic. The broken line represents the prediction from the Stokes–Einstein equation. The coloured solid lines represent the best fitting-lines using eqn (7) and the black solid lines represent the average lines of imidazolium-based and P_{888}-based ILs. The literature values are taken from ref. 17.

D_0 and α for each solute and solvent molecule. The α values for all solvents followed the order CO < DPA < DPCP, which corresponds to the molecular radius hierarchy of the solutes. This result indicates that smaller solute molecules deviate more significantly from the SE rule. Similar tendency has been reported for the diffusion of neutral molecules in molecular solvents and ILs.[17,39–41]

The diffusion coefficients of CO in imidazolium-based ILs exhibited similar behaviour irrespective of the cation species (dicationic or not) and showed negligible dependence on the alkyl chain length. Furthermore, the diffusion coefficients of CO in phosphonium-based DILs were similar to those in $[P_{8888}][NTf_2]$, almost independent of the alkyl linkage chain length. The values were significantly different from those of imidazolium-based ILs. These results could not be explained by the model reported by Kaintz *et al.*,[16] where the diffusion coefficients in ILs deviate from the SE rule with an increase in the relative size of the solute molecule to that of the solvent molecule. Our results imply that the diffusion coefficients of CO are not determined by the alkyl chain length per cation. The van der Waals volumes of the cations estimated using Bondi's method[42] are 161 Å^3 for $[C_5mim]^+$, 212 Å^3 for $[C_{10}mim]^+$, and 315 Å^3 for $[C_{10}(mim)_2]^{2+}$ in the imidazolium-based ILs. The volume of $[C_{10}(mim)_2]^{2+}$ is nearly twice that of $[C_5mim]^+$. For the phosphonium-based ILs, $[P_{8888}]^+$ is estimated to be 582 Å^3, $[(P_{888})_2C_6]^{2+}$ 1054 Å^3, and $[(P_{888})_2C_{10}]^{2+}$ 1095 Å^3. The volumes of the DILs are almost twice those of the monocationic IL; that is, the volume per charge is similar. Therefore, the volume per charge is an important factor that determines the diffusion coefficient of CO, and whether ILs are dicationic is trivial. According to a molecular dynamics simulation study by Margulis *et al.*, the polar and nonpolar parts played different roles in the diffusion of small neutral molecules in ILs.[43,44] Although the solute molecules are subject to high friction in the polar part and retained near the charge centre, leading to slow diffusion, they are accelerated in the nonpolar part, which is more remarkable in the longer alkyl chain.[43] In the case of $[C_8mim][NTf_2]$, the solute molecule is preferably solvated by the nonpolar component.[44] While monocationic ILs used in the previous simulation work have one-alkyl chain on the cation, phosphonium-based ILs used in our study have three long alkyl chains. It is expected that the solute molecules pass through the nonpolar part more frequently than imidazolium-based monocationic ILs during the diffusion process. Therefore, the diffusion coefficient of CO in phosphonium-based ILs may be greater than that in imidazolium-based ILs. Our finding in this study, "volume per charge is an important factor which determines the diffusion coefficient of CO" is not contradictory to previous computational studies.

The molecular radius of DPA slightly differs from that of DPCP, but the deviation of DPA from the SE rule was larger than that of DPCP. In other words, the α value of DPA was smaller than that of DPCP. This difference can be explained by their polarities. DPA is nonpolar because of its symmetry. In contrast, DPCP has a dipole moment originating from the carbonyl group, which is approximately 5.37 D in vacuum calculated using Gaussian 09[45] with B3LYP functional and 6-311+G(d,p) basis set. Because ILs form nanoscale segregations composed of polar and nonpolar parts,[10] DPCP has electrostatic interactions with the polar domains. Hence, DPCP must diffuse while breaking these interactions. However, DPA does not need to do so. The above can also be confirmed from the activation energy of diffusion. The activation energy for diffusion, E_D, is related to the translational diffusion coefficient D and temperature T as:

$$D = A\exp\left(-\frac{E_D}{k_B T}\right) \quad (8)$$

where A is a constant. The E_D values for CO, DPA, and DPCP in each IL were determined from the slopes of Arrhenius plots. As shown in Table 1, E_D for DPCP was larger than that for DPA when compared with the same IL. Considering that DPA and DPCP have almost the same molecular radius, the increment in E_D can be attributed to the intermolecular interaction energy between solvents and solutes. That is, because the interaction between DPA and ILs is poorer than that between DPCP and ILs, the deviation from the SE rule is larger for DPA than for DPCP.

Table 1 The activation energy E_D of each solute molecule

	E_D/kJ mol^{-1}		
ILs	CO	DPA	DPCP
$[C_5mim][NTf_2]$	20.8 ± 0.8	26.7 ± 1.0	29.0 ± 0.5
$[C_{10}mim][NTf_2]$	25.9 ± 1.9	25.8 ± 0.6	34.0 ± 0.8
$[C_{10}(mim)_2][NTf_2]_2$	29.8 ± 0.5	39.2 ± 1.3	46.0 ± 0.9
$[(P_{888})_2C_6][NTf_2]_2$	20.7 ± 0.4	33.8 ± 1.1	39.0 ± 0.5
$[(P_{888})_2C_{10}][NTf_2]_2$	24.2 ± 0.7	30.5 ± 1.6	39.7 ± 0.8
$[P_{4441}][NTf_2]$[a]	22.9 ± 0.7	27.9 ± 0.8	30.6 ± 3.9
$[P_{8888}][NTf_2]$[a]	18.0 ± 0.4	30.5 ± 2.3	35.2 ± 1.4

[a] Calculated from the data taken from ref. 17.

The diffusion coefficients of DPCP exhibited the same behaviour for all the imidazolium-based ILs. In contrast, the diffusion coefficients of phosphonium-based DILs and $[P_{8888}][NTf_2]$ behaved differently. This trend was not observed for the diffusion coefficients of CO, suggesting that for phosphonium-based ILs, whether the ILs are dicationic is a key factor when the solutes are large, such as DPCP (3.54 Å). Notably, this was independent of the alkyl linkage chain length. In terms of molecular radius, similar arguments apply to the diffusion coefficients of DPA (3.50 Å).

5. Conclusions

We synthesized the novel phosphonium-based DILs, $[(P_{888})_2C_n][NTf_2]_2$ (n = 6, 10), and investigated physicochemical properties and translational diffusion of three solute molecules in the DILs. As the alkyl linkage chain increased, the viscosity decreased and the nonpolar domain became small. The TG measurement revealed that the diffusion coefficient of CO was determined not by whether ILs are dicationic, but by the alkyl chain length of the cation per charge centre. Meanwhile, when large neutral molecules such as DPA (3.50 Å) and DPCP (3.54 Å) diffused, the dicationic nature of phosphonium-based ILs was important. The difference in the viscosity dependence of the diffusion coefficients for DPA and DPCP could be explained by their polarities. Our experimental findings of the phosphonium-based DILs will spice up science of ionic liquids and solution chemistry.

Author contributions

S. O. and Y. K. designed the experiments. Y. K. supervised the work. M. F. mainly performed TG experiments and analyses, and viscosity measurements. S. O. synthesized all phosphonium-based ILs (including DILs) and made thermal measurements under the supervision of T. E. S. S., K. O. and T. E. performed X-ray measurements. M. F. and S. O. mainly wrote the manuscript with help and discussion from all authors, particularly Y. K.

Conflicts of interest

There are no conflicts to declare.

Data availability

The data supporting this article have been included as part of the supplementary information (SI). Supplementary information: Tables S1–S9, NMR spectra (Fig. S1 and S2) and further figures for analysis (Fig. S3–S5). See DOI: https://doi.org/10.1039/d5cp04887g.

Acknowledgements

The authors acknowledge Mr So Ueno and Prof. Hiroko Yamada (Kyoto University) for measuring the MS spectra. This study was supported by the Joint Usage/Research Center [JURC, Institute for Chemical Research (ICR), Kyoto University] by providing access to ESI (Bruker timsTOF (IMS-QTOF)). The authors acknowledge Mr Ryo Sato (Doshisha University) for synthesizing $[C_{10}(mim)_2][NTf_2]_2$. This work is partially supported by JSPS KAKENHI (Grant Number 22H02040).

References

1 K. S. Egorova, E. G. Gordeev and V. P. Ananikov, *Chem. Rev.*, 2017, **117**, 7132–7189.
2 J. Dupont and J. D. Scholten, *Chem. Soc. Rev.*, 2010, **39**, 1780–1804.
3 P. Hapiot and C. Lagrost, *Chem. Rev.*, 2008, **108**, 2238–2264.
4 V. I. Pârvulescu and C. Hardacre, *Chem. Rev.*, 2007, **107**, 2615–2665.
5 M. Watanabe, M. L. Thomas, S. Zhang, K. Ueno, T. Yasuda and K. Dokko, *Chem. Rev.*, 2017, **117**, 7190–7239.
6 Y. Wang and G. A. Voth, *J. Am. Chem. Soc.*, 2005, **127**, 12192–12193.
7 J. N. Canongia Lopes and A. A. Padua, *J. Phys. Chem. B*, 2006, **110**, 3330–3335.
8 A. Triolo, O. Russina, H.-J. Bleif and E. Di Cola, *J. Phys. Chem. B*, 2007, **111**, 4641–4644.
9 O. Yamamuro, T. Yamada, M. Kofu, M. Nakakoshi and M. Nagao, *J. Chem. Phys.*, 2011, **135**, 054508.
10 Y. L. Wang, B. Li, S. Sarman, F. Mocci, Z. Y. Lu, J. Yuan, A. Laaksonen and M. D. Fayer, *Chem. Rev.*, 2020, **120**, 5798–5877.
11 S. Li, G. Feng, J. L. Bañuelos, G. Rother, P. F. Fulvio, S. Dai and P. T. Cummings, *J. Phys. Chem. C*, 2013, **117**, 18251–18257.
12 S. Li, J. L. Banuelos, P. Zhang, G. Feng, S. Dai, G. Rother and P. T. Cummings, *Soft Matter*, 2014, **10**, 9193–9200.
13 H. Shirota, T. Mandai, H. Fukazawa and T. Kato, *J. Chem. Eng. Data*, 2011, **56**, 2453–2459.
14 Z. Zhang, L. Yang, S. Luo, M. Tian, K. Tachibana and K. Kamijima, *J. Power Sources*, 2007, **167**, 217–222.
15 Y. Kimura, *Pure Appl. Chem.*, 2020, **92**, 1695–1708.
16 A. Kaintz, G. Baker, A. Benesi and M. Maroncelli, *J. Phys. Chem. B*, 2013, **117**, 11697–11708.
17 Y. Kimura, Y. Kida, Y. Matsushita, Y. Yasaka, M. Ueno and K. Takahashi, *J. Phys. Chem. B*, 2015, **119**, 8096–8103.

18 H. E. Gottlieb, V. Kotlyar and A. Nudelman, *J. Org. Chem.*, 1997, **62**, 7512–7515.
19 H. Miyabayashi, K. Fujii, T. Watanabe, Y. Matano, T. Endo and Y. Kimura, *J. Phys. Chem. B*, 2021, **125**, 5373–5386.
20 K. Ito, N. Nishina and H. Ohno, *Electrochim. Acta*, 2000, **45**, 1295–1298.
21 T. Endo, H. Sumida, T. Nakamura, H. Sugihara and Y. Kimura, *Bull. Chem. Soc. Jpn.*, 2025, **98**, uoaf016.
22 H. Kuramochi, S. Takeuchi and T. Tahara, *Chem. Phys.*, 2018, **512**, 88–92.
23 S. Takeuchi and T. Tahara, *J. Chem. Phys.*, 2004, **120**, 4768–4776.
24 J. J. Hettige, H. K. Kashyap and C. J. Margulis, *J. Chem. Phys.*, 2014, **140**, 111102.
25 T. Cosby, Z. Vicars, M. Heres, K. Tsunashima and J. Sangoro, *J. Chem. Phys.*, 2018, **148**, 193815.
26 K. L. Luska and A. Moores, *Green Chem.*, 2012, **14**, 1736–1742.
27 K. Tsunashima and M. Sugiya, *Electrochem. Commun.*, 2007, **9**, 2353–2358.
28 M. Terazima, *J. Appl. Phys.*, 2022, **131**, 140902.
29 M. Terazima, *Bull. Chem. Soc. Jpn.*, 2023, **96**, 852–871.
30 M. Terazima, T. Hara and N. Hirota, *Chem. Phys. Lett.*, 1995, **246**, 577–582.
31 B. Yao, M. Paluch, M. Dulski, C. Quinn, S. McLaughlin, A. McGrogan, M. Swadzba-Kwasny and Z. Wojnarowska, *J. Phys. Chem. Lett.*, 2023, **14**, 2958–2964.
32 D. E. Smith, *Electrocatalysis in protic and aprotic ionic liquids for energy application*, PhD thesis, University of Nottingham, 2020.
33 R. Yonekura and M. W. Grinstaff, *Phys. Chem. Chem. Phys.*, 2014, **16**, 20608–20617.
34 E. Ben-Naim, Z. A. Daya, P. Vorobieff and R. E. Ecke, *Phys. Rev. Lett.*, 2001, **86**, 1414–1417.
35 D. M. Raymer and D. E. Smith, *Proc. Natl. Acad. Sci. U. S. A.*, 2007, **104**, 16432–16437.
36 Z. Wojnarowska, S. Cheng, B. Yao, M. Swadzba-Kwasny, S. McLaughlin, A. McGrogan, Y. Delavoux and M. Paluch, *Nat. Commun.*, 2022, **13**, 134237.
37 B. Yao, M. Paluch, M. Dulski, C. Quinn, S. McLaughlin, A. McGrogan, M. Swadzba-Kwasny and Z. Wojnarowska, *J. Phys. Chem. Lett.*, 2023, **14**, 2958–2964.
38 H. K. Kashyap, C. S. Santos, H. V. R. Annapureddy, N. S. Murthy, C. J. Margulis and E. W. Castner, Jr, *Faraday Discuss.*, 2012, **154**, 133–143.
39 D. Fennell Evans, T. Tominaga and C. Chan, *J. Solution Chem.*, 1979, **8**, 461–478.
40 D. F. Evans, T. Tominaga and H. T. Davis, *J. Chem. Phys.*, 1981, **74**, 1298–1305.
41 Y. Nishiyama, M. Fukuda, M. Terazima and Y. Kimura, *J. Chem. Phys.*, 2008, **128**, 164514.
42 A. Bondi, *J. Phys. Chem.*, 1964, **68**, 441–451.
43 J. C. Araque, S. K. Yadav, M. Shadeck, M. Maroncelli and C. J. Margulis, *J. Phys. Chem. B*, 2015, **119**, 7015–7029.
44 J. C. Araque and C. J. Margulis, *J. Chem. Phys.*, 2018, **149**, 144503.
45 M. J. Frisch, *et al.*, *Gaussian 09*, Gaussian, Inc., Wallingford CT, 2010.